ASTRONOMY

Dust formation and wind acceleration around the aluminum oxide–rich AGB star W Hydrae

Aki Takigawa,[1]* Takafumi Kamizuka,[2] Shogo Tachibana,[3†] Issei Yamamura[4,5]

Copyright © 2017 The Authors, some rights reserved; exclusive licensee American Association for the Advancement of Science. No claim to original U.S. Government Works. Distributed under a Creative Commons Attribution NonCommercial License 4.0 (CC BY-NC).

Dust grains, formed around asymptotic giant branch (AGB) stars, are accelerated by stellar radiation to drive stellar winds, which supply freshly synthesized nuclides to the Galaxy. Silicate is the dominant dust species in space, but ~40% of oxygen-rich AGB stars are thought to have comparable amounts of aluminum oxide dust. Dust formation and the wind-driving mechanism around these oxygen-rich stars, however, are poorly understood. We report on the spatial distributions of AlO and ^{29}SiO molecules around an aluminum oxide–rich M-type AGB star, W Hydrae, based on observations obtained with the Atacama Large Millimeter/submillimeter Array. AlO molecules were only observed within three stellar radii (R_{star}), whereas ^{29}SiO was distributed in the accelerated wind beyond 5 R_{star} without significant depletion. This strongly suggests that condensed aluminum oxide dust plays a key role in accelerating the stellar wind and in preventing the efficient formation of silicate dust around W Hydrae.

INTRODUCTION

Acceleration of dust grains by radiation pressure from stellar radiation has been proposed as a trigger for ejecting winds from low- to intermediate-mass stars (*1*). Since its discovery (*2*), broad emission at a wavelength of 11 to 12 μm has been observed for many oxygen-rich asymptotic giant branch (AGB) stars and is now widely interpreted to come from amorphous or metastable aluminum oxide (Al_2O_3) dust (*3*, *4*). Aluminum oxide is one of the most refractory dust species, which form in oxygen-rich circumstellar environments, and has been found in meteorites in the form of presolar grains (*5*). It is surprising that circumstellar dust around ~40% of oxygen-rich AGB stars is rich in aluminum oxide (*6*), considering the low abundance ratio of Al to Si (Al/Si ~ 0.08) (*7*). It has remained a significant conundrum as to why aluminum oxide dust is abundant around oxygen-rich AGB stars.

W Hydrae (W Hya) is a semiregular variable star with a period of 389 days located at a distance of 78 pc (*8*, *9*). Mid-infrared observations of W Hya have shown that 50 to 60% of its dust consists of amorphous silicate and one-third of the dust is amorphous aluminum oxide (*10*, *11*). Observations obtained with a near-infrared polarimetric interferometer show that W Hya has a shell of 0.3-μm-radius dust grains at 1.6 to 2.0 R_{star} at the variable phase (ϕ) of 0.2 (*12*). More recently, Ohnaka *et al.* (*13*) showed that W Hya, in its premaximum phase (ϕ = 0.9), has an optically thin dust shell with inner and outer radii of 1.9 to 2.0 R_{star} and 3.0 ± 0.5 R_{star}, respectively, based on visible polarimetric imaging. The dust size was estimated to be 0.1 to 0.5 μm in radius (*13*). Their follow-up observation at minimum light (ϕ = 0.5) confirmed the reality of the dust shell, and they also found newly formed dust at radii up to 10 R_{star}, where 0.1 μm–sized dust is predominant (*14*). These observations suggest that the dust shell consists of aluminum oxide or iron-free silicate, which can exist close to the star, but the dust species has not been identified.

We observed the spatial distributions of AlO and SiO gas molecules around W Hya, because they represent the gas species from which aluminum oxide and silicate dust forms, and they can be useful proxies for dust formation in the stellar outflow. The major isotope of Si is ^{28}Si, but ^{29}SiO was observed to trace the distribution of SiO molecules because ^{28}SiO is expected to be optically too thick near the star and significant isotopic fractionation between ^{28}SiO and ^{29}SiO is not expected during dust formation. Other Al-bearing species such as Al, AlOH, and Al_2O are also important for aluminum oxide formation (*15*), but AlO can trace the dust formation site in the high-temperature region near the star and could be a basic molecule to form aluminum oxide clusters [for example, see the study of van Heijnsbergen *et al.* (*16*)]. So far, AlO molecules have been detected only around an oxygen-rich supergiant, VY Canis Majoris (*15*), Mira variables, specifically *o* Ceti (*17*, *18*), and R Aquarii (*18*) at (sub)millimeter wavelengths.

RESULTS

Long-baseline observations of W Hya with the Atacama Large Millimeter/submillimeter Array (ALMA) (Band 7) were performed on 30 November and 3 and 5 December 2015 (ϕ = 0.3) using 31, 33, and 41 of the 12-m antennas, respectively (see Materials and Methods). The AlO (N = 9–8) line originating from a rotational transition of AlO radicals in the ground electronic state was detected at 344.36 to 344.44 GHz with a frequency resolution of 488.3 kHz channel^{-1} (Fig. 1A). The broad emission feature is consistent with the presence of 12 hyperfine structures of the N = 9–8 transition (Fig. 1A) (*19*). With a beam size of 29 mas (milli–arc sec) × 38 mas, the distribution of AlO (N = 9–8) around W Hya was spatially resolved (Fig. 1B). The emission of the AlO (N = 9–8) transition sharply declined at 50 to 70 mas, and detection at the 3σ confidence level was limited only within ~70 mas (~3 R_{star}) from the star (Fig. 1B). The AlO distribution near the star is surprisingly similar to those of <0.5 μm–sized dust inferred from optical polarized imaging at premaximum and minimum light (ϕ = 0.9 and 0.5; 150 days before and 110 days after the present observation, respectively) (Fig. 1C) (*13*, *14*). This suggests that the dominant dust in the dust shell near the star (2 to 3 R_{star}) consists of aluminum oxide.

The spatially resolved distribution of ^{29}SiO (343.0 GHz, v = 0, J = 8–7) emission was also obtained (Fig. 2) with a beam size of 31 mas × 39 mas. The brightness of the ^{29}SiO line decreased more gradually with distance from the star than that of the AlO emission and extended up

[1]The Hakubi Center for Advanced Research/Division of Earth and Planetary Sciences, Kyoto University, Kitashirakawa Oiwake-cho, Sakyo, Kyoto 606-8502, Japan. [2]Institute of Astronomy, The University of Tokyo, 2-21-1 Osawa, Mitaka, Tokyo 181-0015, Japan. [3]Department of Natural History Science, Hokkaido University, N10W8, Sapporo, Hokkaido 060-0810, Japan. [4]Institute of Space and Astronautical Science, Japan Aerospace Exploration Agency, 3-1-1 Yoshinodai, Chuo-ku, Sagamihara, Kanagawa 252-5210, Japan. [5]Department of Space and Astronautical Science, SOKENDAI, 3-1-1 Yoshinodai, Chuo-ku, Sagamihara, Kanagawa 252-5210, Japan.
*Corresponding author. Email: takigawa@kueps.kyoto-u.ac.jp
†Present address: UTokyo Organization for Planetary and Space Science/Department of Earth and Planetary Science, The University of Tokyo, 7-3-1 Hongo, Tokyo 113-0033, Japan.

Downloaded from http://advances.sciencemag.org/ on November 24, 2017

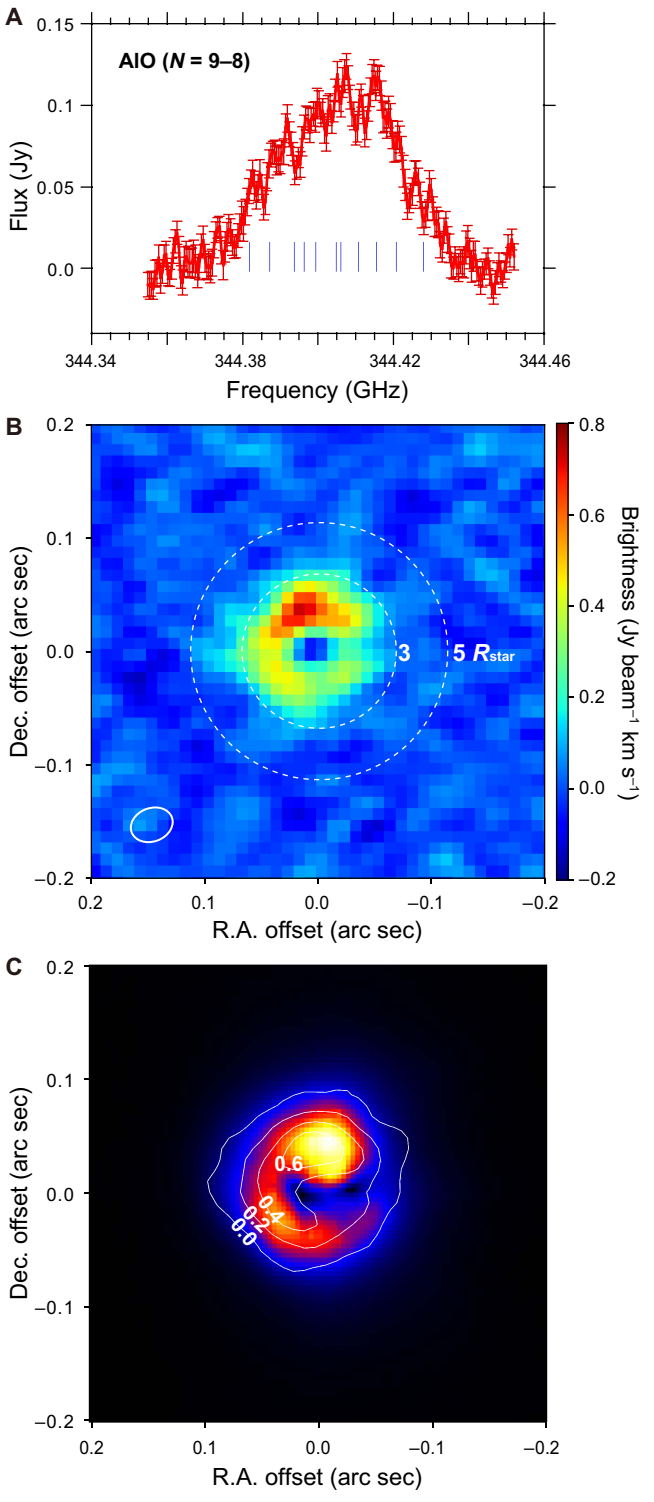

Fig. 1. AlO $N = 9–8$ transition observed around W Hya. (**A**) AlO ($N = 9–8$) line spectrum. Error bars represent the SD obtained in the sky region. The positions of the 12 hyperfine structures of the $N = 9–8$ transition (*19*) at the local standard-of-rest velocity of 40.4 km s^{-1} (*20*) are also indicated (vertical blue lines). (**B**) Continuum-subtracted and integrated AlO intensity map. The open ellipse in the bottom left-hand corner represents the synthesized beam size. The dashed circles show locations at 3 and 5 R_{star} from the star. (**C**) Comparison of the AlO distribution (contours of brightness in units of Jy beam^{-1} km s^{-1}) and a polarized intensity map at 645 nm reflecting the dust distribution (*13*).

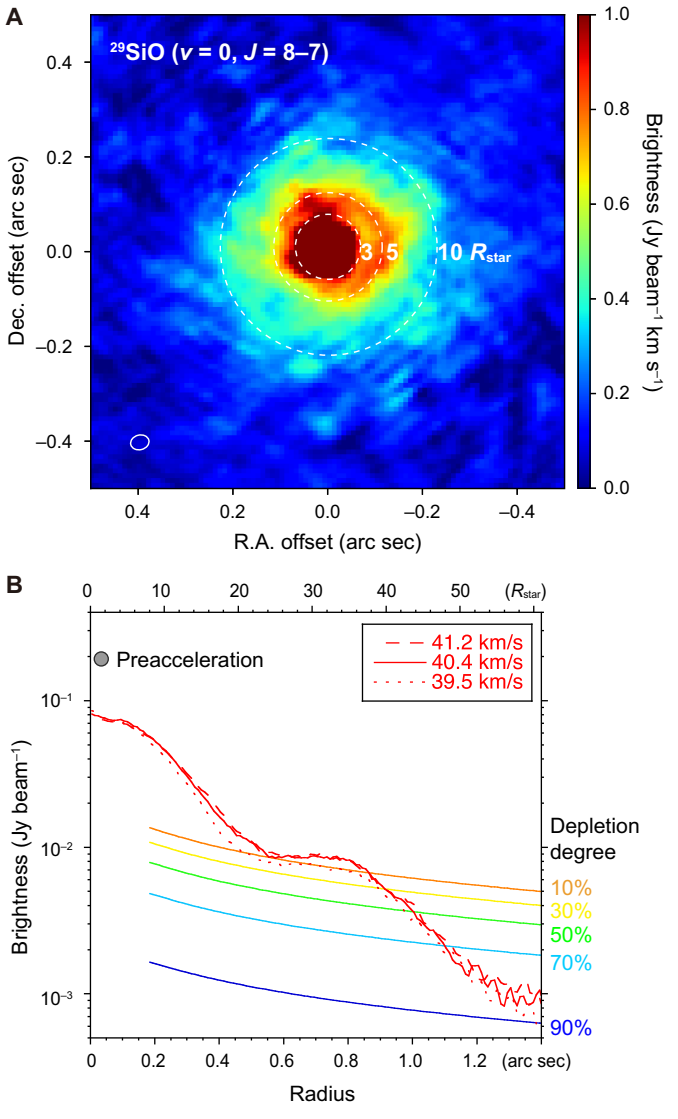

Fig. 2. ^{29}SiO line ($v = 0, J = 8–7$) observed around W Hya. (**A**) Integrated intensity map of ^{29}SiO. The open ellipse in the bottom left-hand corner represents the synthesized beam size. The dashed circles show locations at 3, 5, and 10 R_{star} from the star. (**B**) Annular-averaged line profile of ^{29}SiO at 39.5, 40.4, and 41.2 km s^{-1}. The modeled brightness of ^{29}SiO in the preaccelerated region at 0.07 arc sec (3 R_{star}) is shown by a circle, and the modeled abundance profiles with different degrees of ^{29}SiO depletion (10, 30, 50, 70, and 90%) owing to silicate formation are shown for comparison (see Materials and Methods).

to 0.9 arc sec (~40 R_{star}) from the star at the 3σ confidence level, significantly beyond the AlO distribution (Fig. 2B). The observed SiO molecular distribution (Fig. 2A) covers the region of the newly detected dust at minimum light after our observation (*14*).

Position-velocity diagrams of the ^{29}SiO line ($v = 0, J = 8–7$) along the R.A. (right ascension) and Dec. (declination) axes (Fig. 3) show dark stripes at 35 to 35.8 km s^{-1} due to self-absorption. This suggests that ^{29}SiO molecules are optically thick along the line of sight at this velocity, corresponding to 4.6 to 5.4 km s^{-1} of blueshift relative to the velocity center [40.4 km s^{-1}; (*20*)]. This is most likely caused by an accelerated laminar flow of ^{29}SiO molecules. The 4.6 to 5.4 km s^{-1} blueshift is consistent with the wind velocity of 5.5 km s^{-1} (*11*). Three small blobs with radial velocity

Downloaded from http://advances.sciencemag.org/ on November 24, 2017

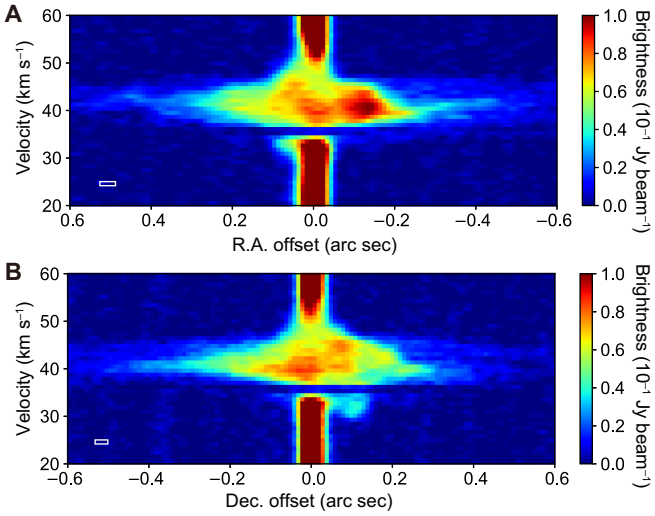

Fig. 3. Position-velocity diagrams of ^{29}SiO line (v = 0, J = 8–7) around W Hya. (**A**) R.A. plane. (**B**) Dec. plane. White rectangles represent the spatial and velocity resolution.

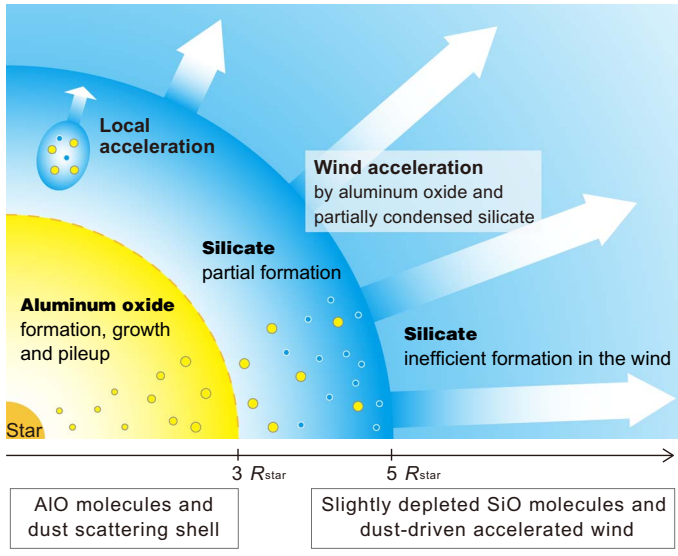

Fig. 4. Dust formation and wind acceleration around W Hya. Aluminum oxide dust, which grows and piles up in the inner dust shell, and partially condensed silicate dust trigger the acceleration of the wind, which suppresses silicate formation around an aluminum oxide–rich star like W Hya.

components of ~43.5 to 45.3 km s^{-1}, which are close to the accelerated expansion velocity of the wind, were also observed at 60 to 85 mas from the star (Fig. 3 and fig. S1).

DISCUSSION

Our ALMA observations show that AlO molecules exist only at ≲3 R_{star} from the star and that their distribution is consistent with the dust distribution observed at both near-maximum and minimum light (Fig. 1C), whereas SiO molecules are present beyond ~3 R_{star} from the star. We obtained an order-of-magnitude estimate of the efficiency of silicate dust formation around W Hya based on a simple radiative transfer model involving the ^{29}SiO line for different acceleration radii R_{acc} (at 2.5 or 5 R_{star}) and different degrees of SiO depletion to silicate dust at R_{cond} (at 2.5 or 5 R_{star}) (see Materials and Methods, Fig. 2B, and fig. S2). The model for R_{acc} = 2.5 R_{star} showed that an abrupt drop of the ^{29}SiO line intensity, by one order of magnitude, should be observed at 2.5 to 5 R_{star} from the star owing to wind acceleration even without silicate dust formation, which is not the case for the present observation (fig. S2). The relatively flat line profile at <5 R_{star} (Fig. 2B) can be reproduced for R_{acc} = 5 R_{star} (fig. S2). This comparison shows that the overall wind acceleration does not occur inside the dust shell observed within 3 R_{star} but occurs beyond the dust shell.

The ^{29}SiO line intensity decreases with distance from the star because of expansion, but it should further decrease if a fraction of SiO molecules condense as silicate dust. A comparison of the decrease of the observed line intensity and that modeled for different degrees of silicate formation (R_{cond} = R_{acc} = 5 R_{star}) suggests that the observed decrease between 70 and 500 mas (3 to 22 R_{star}) can be explained only when <30% of SiO molecules are depleted from gas owing to silicate formation (see Fig. 2B and Materials and Methods). Although more detailed model analysis is necessary to obtain a more quantitative estimate, it is clear that silicate dust does not form effectively in W Hya's accelerated wind and that SiO molecules remain in the gas phase, as observed in this study. The inefficient silicate formation is consistent with the silicate–to–aluminum oxide ratio estimated from mid-infrared dust emission, where only ~6% of the Si atoms should condense as silicate dust if all Al exists in the form of aluminum oxide (*11*).

Because the radial profile of the ^{29}SiO line intensity is consistent with inefficient silicate formation, the dominant dust species in the dust shell at <3 R_{star} observed at ϕ = 0.9 and 0.5 (*13*, *14*) is most likely aluminum oxide. This has been proposed based on mid-infrared (8 to 13 μm) interferometric observations (*21*, *22*). The well-matched spatial distribution of AlO with the dust shell (Fig. 1C) also supports the predominance of aluminum oxide dust in the high-temperature region near the star.

The dust mass in the dust shell within 3.0 R_{star}, observed at different phases both before and after our observation, is estimated at 0.5 × 10^{-9} to 1.0 × 10^{-9} M_{Sun} if the dust is composed of aluminum oxide or silicate (*11*, *14*, *23*). If all Al atoms condense to dust, the mass of aluminum oxide formed within a year is ~2 × 10^{-11} M_{Sun}, assuming the solar elemental abundance and a total mass-loss rate of 1.3 × 10^{-7} M_{Sun} year^{-1} (*21*). This indicates that condensed aluminum oxide dust must pile up in the dust shell over several tens of pulsation cycles. The presence of aluminum oxide dust over multiple pulsation cycles would be sufficient to grow the dust to submicrometer size (*24*), which is comparable to the size estimated from dust scattering (*13*, *14*) (Fig. 4). The survival and growth of aluminum oxide dust near the star is likely possible because of its refractory nature and transparency to the stellar flux (*24*). Once the aluminum oxide grains become larger than ~0.1 μm and their number density increases because of the pileup, they effectively gain momentum through absorption and scattering of stellar photons (*12*, *24*–*26*) and may contribute to wind acceleration.

The SiO blobs we observed (Fig. 3) could be the evidence of wind acceleration by aluminum oxide dust because of the following reasons. (i) The blobs are located 2.3 to 3.3 R_{star} away from the star if we take the face value of the redshift of 3.1 to 4.9 km s^{-1}, whereas they are located 4.3 to 6.1 R_{star} away from the star if the actual velocity of the blobs is the same as the wind expansion velocity of 5.5 km s^{-1} (*11*). These two cases give the lower and upper limits of the blob locations, respectively, and the estimated blob locations (2.3 to 6.1 R_{star} from the star) are within the

Downloaded from http://advances.sciencemag.org/ on November 24, 2017

dust shell or slightly farther beyond the dust shell. (ii) The mass and spatial distribution of the dust shell did not change significantly before and after our observation (*13*, *14*), and the predominance of aluminum oxide dust in the dust shell requires dust accumulation in a relatively stationary extended stellar atmosphere. These features of the dust shell suggest that the extended atmosphere of W Hya is quasi-stationary. (iii) The relatively large velocities of the blobs (3.1 to 5.5 km s^{-1}) should thus be the result of partial acceleration of gas within or near the dust shell, and the most likely driver of acceleration is the stellar radiation on aluminum oxide dust probably because of the locally enhanced dust density (Fig. 4). The present observation therefore strongly suggests that aluminum oxide dust can be a wind accelerator, contrary to the widely accepted view (*26*).

Besides the local wind acceleration near the dust shell, the overall wind acceleration occurs beyond the aluminum oxide dust shell (Fig. 2), which suggests that silicate dust condensing outside the aluminum oxide dust shell also contributes to the acceleration. The contribution of silicate dust to wind acceleration in this star, however, should not be fully significant because the observed SiO distribution implies inefficient silicate formation. Because larger and more concentrated aluminum oxide dust caused by pileup is present in the silicate-forming environment, a small addition of silicate dust to the preexisting aluminum oxide dust may be enough to trigger the overall wind acceleration (Fig. 4). The wind acceleration decreases the gas density, which would suppress further formation of silicate dust in the accelerated wind and explain the aluminum oxide dust–rich nature of W Hya (Fig. 4).

MATERIALS AND METHODS

Observation and data reduction

Observations of W Hya, located at R.A. = $13^h49^m01^s.9981$, Dec. = −28°22′03.488″ (J2000), were carried out for a total of ~4 hours over three separate scheduling blocks executed between 30 November and 5 December 2015 with ALMA in Cycle 3 (Project ID: 2015.1.01446.S). The number of antennas used during each observation block was 31, 33, and 41, respectively, in an extended array configuration. The baselines were 15 m to 8.3 km. Data obtained during these 3 days were calibrated and combined by running calibration scripts provided by the observatory and flagging some additional antennas. A quasar, J1337-1257, was used as a calibrator for flux and bandpass calibration. A second quasar, J1351-2912, was also observed for phase calibration. Because the three observations were performed within a week of each other, the flux of the calibrator was assumed to be constant, and flux equalization was applied to the fluxes on the second observation day, which was characterized by the lowest precipitable water vapor, PWV = 0.63 mm.

Three frequency ranges were covered within ALMA Band 7: 330.4 to 331.3 GHz, 342.4 to 343.3 GHz, and 344.0 to 345.9 GHz. The frequency resolutions were 976.562 kHz $channel^{-1}$ for the first two frequency ranges and 488.281 kHz $channel^{-1}$ for the third range. The ^{29}SiO (342.98 GHz, J = 8–7) and AlO (344.45 GHz, N = 9–8) lines were covered by the second and third frequency ranges, respectively.

Images of AlO and ^{29}SiO were obtained by using CLEAN tasks in CASA version 4.5.0. The standard CLEAN method (*27*) with a circular clean mask with a diameter of 2 arc sec centered at the star was applied to the AlO data, whereas the multiscale CLEAN method (*28*) was applied to clean the extended ^{29}SiO emission. A circular clean mask with a diameter of 3.5 arc sec was applied, and multiscale parameters, which define the full widths at half maximum of clean components in the multiscale CLEAN method, were set to 0, 50, 100, 300, and 600 mas. For visibility weighting, the Briggs mode with a robustness parameter of 0.5 was applied to both data sets. The AlO and ^{29}SiO data were cleaned to flux levels of 5 and 10 millijansky (mJy) $beam^{-1}$, respectively (background noise levels were ~2 mJy $beam^{-1}$). The synthesized pixel size was 10 mas $pixel^{-1}$, and the resulting beam sizes were 29 mas × 38 mas and 31 mas × 39 mas for the AlO and ^{29}SiO images, respectively. The channel map of the ^{29}SiO emission is shown in fig. S1. Continuum subtraction was applied to the AlO image to derive the faint AlO emission around the bright central star. Integrated intensity (moment 0) maps of AlO and ^{29}SiO were obtained by integrating them over 8.5 to 76 km s^{-1} (Figs. 1B and 2A). The noise level for the AlO image was evaluated at 40 mJy $beam^{-1}$ km s^{-1}, corresponding to the root mean square value in a blank sky region, and that for the ^{29}SiO image was 32 mJy $beam^{-1}$ km s^{-1}. Systematic uncertainties of the brightness in the cleaned maps caused by the CLEAN analysis were also evaluated by comparing the images cleaned by different ways. For the AlO image, a comparison with an image cleaned with interactive masking was made, and the ^{29}SiO image was compared with that synthesized by the standard CLEAN method. On the basis of the brightness difference of these images, the systematic brightness uncertainty was estimated to be around 5%.

Radiative transfer model

We carried out a simple radiative transfer calculation of ^{29}SiO emission in the envelope of W Hya to assess the effects of wind acceleration and SiO depletion to silicate dust. A stellar radius of $R_{star} = 3 \times 10^{11}$ m and a distance of 78 pc were adopted (*9*). A spherical envelope with a constant mass-loss rate was assumed. The silicate condensation radius was set at R_{cond} = 2.5 or 5 R_{star}, where the number density of ^{29}SiO was depleted to different degrees (10, 30, 50, 70, and 90%). The wind acceleration location was independently set at R_{acc} = 2.5 or 5 R_{star}. A random turbulent velocity of 1.4 km s^{-1} was assumed for the gas inside R_{acc}, whereas a terminal expansion velocity of 5.5 km s^{-1} with a random motion of 1.4 km s^{-1} was adopted for the gas beyond R_{acc} (*21*). The mass-loss rate was set at 1.3×10^{-7} M_{Sun} $year^{-1}$ (*21*). The outer edge of the SiO envelope was set at 100 R_{star} (*29*). The temperature profiles of the dust and gas were given by $T_{dust}(r) = 2500 \times (r/R_{star})^{-0.4}$ and $T_{gas}(r) = 2500 \times (r/R_{star})^{-0.65}$, respectively. A local thermodynamical equilibrium was assumed to calculate the SiO intensity profile. Line frequency and dipole moment of SiO were taken from Glenar *et al.* (*30*) and Langhoff and Bauschlicher (*31*), respectively, and the warm silicate opacity by Ossenkopf *et al.* (*32*) was adopted for dust continuum. The result was expressed as a two-dimensional channel map and converted to the observational image by a simple convolution with a Gaussian profile, which has the same size and position angle as the observation beam. The resolve-out effect is expected to be insignificant because the size of the ^{29}SiO shell [~5.1 arc sec in diameter; (*29*)] is smaller than the maximum recoverable scale of our observations (7.2 arc sec).

Comparison of the radial distributions of the observed and modeled ^{29}SiO emission (fig. S2) shows that regardless of the depletion degree, the models with R_{acc} = 2.5 R_{star} cannot reproduce the relatively flat pattern of the brightness observed at <5 R_{star}. The comparison also indicates that the degree of ^{29}SiO depletion should be less than 30%, irrespective of R_{acc} and R_{cond}, to reproduce the observed brightness at 0.5 to 0.8 arc sec (~10^{-2} Jy $beam^{-1}$).

Downloaded from http://advances.sciencemag.org/ on November 24, 2017

SUPPLEMENTARY MATERIALS

Supplementary material for this article is available at http://advances.sciencemag.org/cgi/content/full/3/11/eaao2149/DC1

fig. S1. Channel map of the ^{29}SiO for different velocities.

fig. S2. Radial distribution of modeled ^{29}SiO emission.

REFERENCES AND NOTES

1. E. Sedlmayr, C. Dominik, Dust driven winds. *Space Sci. Rev.* **73**, 211–272 (1995).
2. I. R. Little-Marenin, S. D. Price, *The Shapes of the Circumstellar Silicate Features* (Ames Research Center Summer School on Interstellar Processes: Abstracts of Contributed Papers, NASA, 1986), 137–138.
3. T. Onaka, T. de Jong, F. J. Willems, A study of M Mira variables based on IRAS LRS observations. I. Dust formation in the circumstellar shell. *Astron. Astrophys.* **218**, 169–179 (1989).
4. A. K. Speck, M. J. Barlow, R. J. Sylvester, A. M. Hofmeister, Dust features in the 10-μm infrared spectra of oxygen-rich evolved stars. *Astron. Astrophys. Suppl. Ser.* **146**, 437–464 (2000).
5. A. Takigawa, S. Tachibana, G. R. Huss, K. Nagashima, K. Makide, A. N. Krot, H. Nagahara, Morphology and crystal structures of solar and presolar Al_2O_3 in unequilibrated ordinary chondrites. *Geochim. Cosmochim. Acta* **124**, 309–327 (2014).
6. G. C. Sloan, K. E. Kraemer, J. H. Goebel, S. D. Price, Guilt by association: The 13 micron dust emission feature and its correlation to other gas and dust features. *Astrophys. J.* **594**, 483–495 (2003).
7. K. Lodders, Solar system abundances and condensation temperatures of the elements. *Astrophys. J.* **591**, 1220–1247 (2003).
8. S. Uttenthaler, K. Van Stiphout, K. Voet, H. Van Winckel, S. Van Eck, A. Jorissen, F. Kerschbaum, G. Raskin, S. Prins, W. Pessemier, C. Waelkens, Y. Frémat, H. Hensberge, L. Dumortier, H. Lehmann, The evolutionary state of Miras with changing pulsation periods. *Astron. Astrophys.* **531**, A88 (2011).
9. G. R. Knapp, D. Pourbaix, I. Platais, A. Jorissen, Reprocessing the Hipparcos data of evolved stars. III. Revised Hipparcos period–luminosity relationship for galactic long-period variable stars. *Astron. Astrophys.* **403**, 993–1002 (2003).
10. A. M. Heras, S. Hony, Oxygen-rich AGB stars with optically thin dust envelopes. *Astron. Astrophys.* **439**, 171–182 (2005).
11. T. Khouri, A. de Koter, L. Decin, L. B. F. M. Waters, M. Maercker, R. Lombaert, J. Alcolea, J. A. D. L. Blommaert, V. Bujarrabal, M. A. T. Groenewegen, K. Justtanont, F. Kerschbaum, M. Matsuura, K. M. Menten, H. Olofsson, P. Planesas, P. Royer, M. R. Schmidt, R. Szczerba, D. Teyssier, J. Yates, The wind of W Hydrae as seen by *Herschel*. II. The molecular envelope of W Hydrae. *Astron. Astrophys.* **570**, A67 (2014).
12. B. R. M. Norris, P. G. Tuthill, M. J. Ireland, S. Lacour, A. A. Zijlstra, F. Lykou, T. M. Evans, P. Stewart, T. R. Bedding, A close halo of large transparent grains around extreme red giant stars. *Nature* **484**, 220–222 (2012).
13. K. Ohnaka, G. Weigelt, K.-H. Hofmann, Clumpy dust clouds and extended atmosphere of the AGB star W Hydrae revealed with VLT/SPHERE-ZIMPOL and VLTI/AMBER. *Astron. Astrophys.* **589**, A91 (2016).
14. K. Ohnaka, G. Weigelt, K.-H. Hofmann, Clumpy dust clouds and extended atmosphere of the AGB star W Hydrae revealed with VLT/SPHERE-ZIMPOL and VLTI/AMBER. *Astron. Astrophys.* **597**, A20 (2017).
15. E. D. Tenenbaum, L. M. Ziurys, Millimeter detection of AlO ($X^2\Sigma^+$): Metal oxide chemistry in the envelope of VY canis majoris. *Astrophys. J. Lett.* **694**, L59–L63 (2009).
16. D. van Heijnsbergen, K. Demyk, M. A. Duncan, G. Meijer, G. von Helden, Structure determination of gas phase aluminum oxide clusters. *Phys. Chem. Chem. Phys.* **5**, 2515–2519 (2003).
17. T. Kamiński, K. T. Wong, M. R. Schmidt, H. S. P. Müller, C. A. Gottlieb, I. Cherchneff, K. M. Menten, D. Keller, S. Brünken, J. M. Winters, N. A. Patel, An observational study of dust nucleation in Mira (o Ceti). I. Variable features of AlO and other Al-bearing species. *Astron. Astrophys.* **592**, A42 (2016).
18. E. De Beck, L. Decin, S. Ramstedt, H. Olofsson, K. M. Menten, N. A. Patel, W. H. T. Vlemmings, Search for aluminium monoxide in the winds of oxygen-rich AGB stars. *Astron. Astrophys.* **598**, A53 (2017).
19. C. Yamada, E. A. Cohen, M. Fujitake, E. Hirota, The microwave spectrum of the AlO radical. *J. Chem. Phys.* **92**, 2146–2149 (1990).
20. T. Khouri, A. de Koter, L. Decin, L. B. F. M. Waters, R. Lombaert, P. Royer, B. Swinyard, M. J. Barlow, J. Alcolea, J. A. D. L. Blommaert, V. Bujarrabal, J. Cernicharo, M. A. T. Groenewegen, K. Justtanont, F. Kerschbaum, M. Maercker, A. Marston, M. Matsuura, G. Melnick, K. M. Menten, H. Olofsson, P. Planesas, E. Polehampton, Th. Posch, M. Schmidt, R. Szczerba, B. Vandenbussche, J. Yates, The wind of W Hydrae as seen by *Herschel*. I. The CO envelope. *Astron. Astrophys.* **561**, A5 (2014).
21. R. Zhao-Geisler, A. Quirrenbach, R. Köhler, B. Lopez, C. Leinert, The mid-infrared diameter of W Hydrae. *Astron. Astrophys.* **530**, A120 (2011).
22. R. Zhao-Geisler, R. Köhler, F. Kemper, F. Kerschbaum, A. Mayer, A. Quirrenbach, B. Lopez, Spectro-imaging of the asymmetric inner molecular and dust shell region of the Mira variable W Hya with MIDI/VLTI. *Publ. Astron. Soc. Pac.* **127**, 732–741 (2015).
23. T. Khouri, L. B. F. M. Waters, A. de Koter, L. Decin, M. Min, B. L. de Vries, R. Lombaert, N. L. J. Cox, Dusty wind of W Hydrae. Multi-wavelength modelling of the present-day and recent mass loss. *Astron. Astrophys.* **577**, A114 (2015).
24. D. Gobrecht, I. Cherchneff, A. Sarangi, J. M. C. Plane, S. T. Bromley, Dust formation in the oxygen-rich AGB star IK Tauri. *Astron. Astrophys.* **585**, A6 (2016).
25. S. Höfner, Winds of M-type AGB stars driven by micron-sized grains. *Astron. Astrophys.* **491**, L1–L4 (2008).
26. S. Höfner, S. Bladh, B. Aringer, R. Ahuja, Dynamic atmospheres and winds of cool luminous giants. I. Al_2O_3 and silicate dust in the close vicinity of M-type AGB stars. *Astron. Astrophys.* **594**, A108 (2016).
27. J. A. Högbom, Aperture synthesis with a non-regular distribution of interferometer baselines. *Astron. Astrophys. Suppl. Ser.* **15**, 417–426 (1974).
28. T. J. Cornwell, Multiscale CLEAN deconvolution of radio synthesis images. *IEEE J. Sel. Top. Signal Process.* **2**, 793–801 (2008).
29. D. González Delgado, H. Olofsson, F. Kerschbaum, F. L. Schöier, M. Lindqvist, M. A. T. Groenewegen, "Thermal" SiO radio line emission towards M-type AGB stars: A probe of circumstellar dust formation and dynamics. *Astron. Astrophys.* **411**, 123–147 (2003).
30. D. A. Glenar, A. R. Hill, D. E. Jennings, J. W. Brault, Vibration-rotation parameters for high-temperature silicon monoxide from sunspot spectra. *J. Mol. Spectrosc.* **111**, 403–414 (1985).
31. S. R. Langhoff, C. W. Bauschlicher Jr., A theoretical study of the electric dipole moment function of SiO. *Chem. Phys. Lett.* **211**, 305–311 (1993).
32. V. Ossenkopf, Th. Henning, J. S. Mathis, Constraints on cosmic silicates. *Astron. Astrophys.* **261**, 567–578 (1992).

Acknowledgments: We thank K. Ohnaka and the ALMA star working group for valuable discussions, and F. Egusa, A. Kawamura, and the ALMA staff for their support of the observations and data analysis. Data analysis was carried out on the open use data analysis computer system at the Astronomy Data Center of the National Astronomical Observatory of Japan (NAOJ). **Funding:** This work was supported by Japan Society for the Promotion of Science KAKENHI (grants JP12J02495 and JP15K17787 to A.T.). **Author contributions:** A.T. designed and directed the study. T.K. carried out the data reduction. I.Y. made the radiative transfer model. S.T. discussed the data. A.T. wrote the manuscript. All authors commented on the paper. **Competing interests:** The authors declare that they have no competing interests. **Data and materials availability:** This paper makes use of the following ALMA data: ADS/JAO.ALMA#2015.1.01446.S. ALMA is a partnership of European Southern Observatory (ESO) (representing its member states), NSF (United States), and National Institutes of Natural Sciences (Japan), together with National Research Council (Canada), Ministry of Science and Technology and Academia Sinica Institute of Astronomy and Astrophysics (Taiwan), and Korea Astronomy and Space Science Institute (Republic of Korea), in cooperation with the Republic of Chile. The Joint ALMA Observatory is operated by ESO, Associated Universities, Inc./National Radio Astronomy Observatory, and NAOJ. The data used in this study are available from the ALMA Science Archive (https://almascience.nrao.edu/aq/). Additional data related to this paper may be requested from the authors.

Submitted 26 June 2017
Accepted 4 October 2017
Published 1 November 2017
10.1126/sciadv.aao2149

Citation: A. Takigawa, T. Kamizuka, S. Tachibana, I. Yamamura, Dust formation and wind acceleration around the aluminum oxide–rich AGB star W Hydrae. *Sci. Adv.* **3**, eaao2149 (2017).

Downloaded from http://advances.sciencemag.org/ on November 24, 2017

Science Advances

Dust formation and wind acceleration around the aluminum oxide–rich AGB star W Hydrae

Aki Takigawa, Takafumi Kamizuka, Shogo Tachibana and Issei Yamamura

Sci Adv **3** (11), eaao2149.
DOI: 10.1126/sciadv.aao2149

ARTICLE TOOLS http://advances.sciencemag.org/content/3/11/eaao2149

SUPPLEMENTARY MATERIALS http://advances.sciencemag.org/content/suppl/2017/10/30/3.11.eaao2149.DC1

REFERENCES This article cites 31 articles, 0 of which you can access for free
http://advances.sciencemag.org/content/3/11/eaao2149#BIBL

PERMISSIONS http://www.sciencemag.org/help/reprints-and-permissions

Use of this article is subject to the Terms of Service

Science Advances (ISSN 2375-2548) is published by the American Association for the Advancement of Science, 1200 New York Avenue NW, Washington, DC 20005. 2017 © The Authors, some rights reserved; exclusive licensee American Association for the Advancement of Science. No claim to original U.S. Government Works. The title *Science Advances* is a registered trademark of AAAS.

Downloaded from http://advances.sciencemag.org/ on November 24, 2017